

# Large-scale shocks in the starburst galaxy NGC 253

## Interferometer mapping of a $\sim 600$ pc SiO/H<sup>13</sup>CO<sup>+</sup> circumnuclear disk

S. García-Burillo<sup>1</sup>, J. Martín-Pintado<sup>1</sup>, A. Fuente<sup>1</sup>, and R. Neri<sup>2</sup>

<sup>1</sup> Observatorio Astronómico Nacional (IGN), Apartado 1143, 28800 Alcalá de Henares, Madrid, Spain (burillo, martin, fuente@oan.es)

<sup>2</sup> IRAM-Institut de Radio Astronomie Millimétrique, 300 Rue de la Piscine, 38406 St. Mt. d'Hères, France (neri@iram.fr)

Received 22 July 1999 / Accepted 4 January 2000

**Abstract.** This paper presents the first high-resolution SiO map made in an external galaxy. The nucleus of the nearby barred spiral NGC 253 has been observed simultaneously in the  $v=0$ ,  $J=2-1$  line of SiO and in the  $J=1-0$  line of H<sup>13</sup>CO<sup>+</sup> with the IRAM interferometer, with a resolution of  $7.5'' \times 2.6''$ .

Emission from SiO and H<sup>13</sup>CO<sup>+</sup> is extended in the nucleus of NGC 253. The bulk of the SiO/H<sup>13</sup>CO<sup>+</sup> emission arises from a ( $600\text{pc} \times 250\text{pc}$ ) circumnuclear disk (CND) with a double ringed structure. The inner ring, of radius  $r \sim 60\text{pc}$  ( $4''$ ), viewed edge-on along  $\text{PA} = 51^\circ$ , hosts the nuclear starburst; the outer pseudo-ring opens out as a spiral-like arc up to  $r \sim 300\text{pc}$  ( $20''$ ). The kinematics of the gaseous disk, characterized by strong non-circular motions, is interpreted in terms of the resonant response of the gas to the barred potential. The inner ring would correspond to the inner Inner Lindblad Resonance (iILR), whereas the outer region is linked to the onset of a trailing spiral wave across the outer ILR (oILR). This scenario accounts for the unlike morphology of the maps observed in different molecules.

Most notably, we report the detection of a molecular gas counterpart of the giant outflow of hot gas, previously seen in X-ray and optical lines, and tentatively identified as a dust chimney in the the  $450\mu$  continuum band. Two gas filaments appear in the SiO map to come out of the plane in the NGC 253 nucleus at  $r \pm 60\text{pc}$ , delimiting the working surfaces of gas entrained by the hot wind.

The SiO shows a high average fractional abundance in the CND of  $\langle X(\text{SiO}) \rangle \sim 1.5 \times 10^{-10}$ . This is more than an order of magnitude above the predicted value of a PDR. Moreover,  $X(\text{SiO})$  varies at least by an order of magnitude between the inner starburst region, which dominates the global emission, where we derive  $X(\text{SiO}) \sim 1-2 \times 10^{-10}$ , and the outer region, where  $X(\text{SiO})$  reaches a few  $10^{-9}$ . SiO abundance is also significantly enhanced in the outflow ( $X(\text{SiO}) \sim 3-5 \times 10^{-10}$ ). Different mechanisms are explored to explain the unlike chemical processing of molecular gas within the nucleus. Large-scale shocks induced by the crowding of clouds orbits across the oILR in the outer region and by the outflow of hot gas seem to be by large the most efficient mechanisms in rising the Silicon abundance.

**Key words:** galaxies: individual: NGC 253 – galaxies: ISM – galaxies: kinematics and dynamics – galaxies: spiral

### 1. Introduction

Among all tracers of the high density gas in spirals, the SiO molecule presents the most peculiar, and so far, poorly understood chemistry. Galactic surveys of SiO clouds show that the relative abundance of this species varies by more than five orders of magnitude (the relative abundance,  $X(\text{SiO})$ , ranges from  $< 10^{-12}$  to  $10^{-7}$ ). SiO emission is practically absent in quiescent dark clouds, indicating a high degree of depletion in grains as  $X(\text{SiO}) \sim$  a few  $10^{-12}$  (Ziurys et al. 1989). In contrast, SiO is enhanced in the dense and hot gas of GMCs forming massive stars, in particular, it appears in association with bipolar outflows where  $X(\text{SiO}) \sim 10^{-7}-10^{-8}$  (Martín-Pintado et al. 1992, Schilke et al. 1997, Gueth et al. 1998). These high abundances have been interpreted as a signature of shock chemistry: SiO comes into the gas phase by the sputtering of grains by fast shocks. At significantly lower abundances ( $X(\text{SiO}) \sim 10^{-11}-10^{-10}$ ), SiO is predicted in Photon-Dominated-Regions (PDRs), complexes of molecular gas heated by UV photons produced by OB associations (Janssen et al. 1995, Walmsley et al. 1999). Finally, SiO emission has been reported in molecular clouds of the Galactic Center with  $X(\text{SiO}) \sim 10^{-8}-10^{-9}$  (Martín-Pintado et al. 1997, Hüttemeister et al. 1998). However these clouds show little evidence of recent star formation. The emission in these clouds might be connected with large-scale shocks rather than with star formation. Shocks are possibly driven by the bar potential or, more locally, by superbubbles and supernova remnants.

SiO emission was first detected in NGC 253 by Mauersberger and Henkel (1991). A later study by Sage and Ziurys (1995) reported the detection of  $J=2-1$  SiO emission in several starburst galaxies, including NGC 253. The authors concluded that the ratio  $I(\text{SiO})/I(\text{N}_2\text{H}^+)$  is an indicator of the SFR per unit mass. However, their conclusions on the origin of SiO emission are based on low resolution observations of only one transition. With the aim of studying the physical and the chemical parameters of SiO clouds, we mapped in the  $J=5-4$ ,  $3-2$  and  $2-1$  transitions of SiO the nuclei of three prototypical starbursts:

M 82, NGC 253 and IC 342 (Martín-Pintado et al. 1999, hereafter called **MP99**). First results of our survey, made with the 30m telescope, underlined the different influence of star formation in these galaxies. First, the inferred SiO abundances were seen to vary from galaxy to galaxy (from  $X(\text{SiO}) \sim 10^{-8}$  in IC 342 to  $\sim 10^{-10}$  in M 82), showing no correlation with changes on the SFR per unit mass. Physical conditions of SiO clouds, derived from the transition ratios, are also markedly different in our sample.

However, any further refinement in the interpretation of SiO emission required a better angular resolution. In particular, it is crucial to elucidate which is the exact spatial extent of SiO emission in the nuclei of starburst galaxies. So far it is unclear if SiO emission is exclusively linked with the formation of massive stars, or alternatively, with the occurrence of large-scale shocks, as observations of clouds in our Galaxy seem to indicate. We want to address the question of which is the chemical scenario explaining the abundance of SiO in galaxies.

In this paper we study at high-resolution the SiO( $v=0, J=2-1$ ) emission in the nucleus of NGC 253, a highly inclined barred Sc spiral representing the archetype of a nuclear starburst. The bulk of its large infrared luminosity  $L_{IR} \sim 1.6 \times 10^{10} L_{\odot}$  originates in the inner 300 pc (Telesco and Harper 1980). The observed infrared spectrum of the nucleus (Telesco and Harper 1980; Engelbracht et al. 1998) as well as the radio continuum observations made at centimeter wavelengths (Antonucci and Ulvestad 1988, Ulvestad and Antonucci 1991) support the starburst hypothesis. There is also evidence of a giant outflow of hot gas powered by the starburst, that comes out of the galaxy plane (Fabbiano and Trinchieri 1984, McCarthy et al. 1987, Schulz and Wegner 1992). The high molecular gas mass of the NGC 253's nucleus ( $\sim 2-3 \times 10^8 M_{\odot}$ ; Canzian et al. 1988; Mauersberger et al. 1996) explains the high SFR. Water maser emission detected by Ho et al. (1987) reveals strong star formation activity. The gas reservoir might have been driven inward by the barred potential first identified by Scoville et al. (1985) in a K-band image of the galaxy. Several interferometer maps showing the molecular gas distribution of NGC 253's nucleus have been published (CO: Canzian et al. 1988; HCN: Paglione et al. 1995; CN: Hüttemeister and Aalto 1998, HCO<sup>+</sup>: Carlstrom et al. 1990; OH: Turner 1985; H<sub>2</sub>CO: Baan et al. 1997; CS: Peng et al. 1996, hereafter **P96**) However, no high-resolution image of the dense gas distribution ( $n(\text{H}_2) > 10^5 \text{ cm}^{-3}$ ) has been obtained so far, using an optically thin tracer. To fill this gap, we have made simultaneous observations in the  $J=1-0$  line of H<sup>13</sup>CO<sup>+</sup>, a tracer of dense gas with low opacity. Furthermore all the results for SiO and H<sup>13</sup>CO<sup>+</sup> are discussed in parallel throughout the paper. In particular we study how the ratio of integrated intensities  $I(\text{SiO})/I(\text{H}^{13}\text{CO}^+)$  changes across the nucleus and discuss how this result is used to get the variation of the absolute abundance of SiO.

## 2. Observations

Observations of NGC 253 were made with the IRAM array at Plateau de Bure (France) between June and August 1998.

We simultaneously observed the ( $v=0, J=2-1$ ) line of SiO (at 86.847 GHz) and the ( $J=1-0$ ) line of H<sup>13</sup>CO<sup>+</sup> (at 86.754 GHz) using the standard BC set of 4-antenna configurations. The 55'' primary beam field of the interferometer was phase-centered at  $\alpha_{J2000}=00^{\text{h}}47^{\text{m}}33.0^{\text{s}}$  and  $\delta_{J2000}=-25^{\circ}17'18.4''$ .

The SIS receivers were tuned for single side band operation at 86.731 GHz yielding system temperatures of 100 – 200 K. The spectral correlator was adjusted to give a contiguous bandwidth of 420 MHz. This is equivalent to a velocity range of 1500  $\text{km s}^{-1}$ ; the correlator was centered at 86.731 GHz in order to cover both transitions. The effective frequency resolution was set to 2.5 MHz, or equivalently 8.64  $\text{km s}^{-1}$  at this frequency.

Visibilities were obtained using on-source integration times of 20 minutes interspersed with 4 minutes of instrumental amplitude and phase calibrations. These were made by observing 0135-247 and 2345-167. The atmospheric phase noise on the most extended baselines ranged from 20° to 40°, consistent with a seeing of 0.8–1.2'', typical for summer weather conditions. The absolute flux density scale was established on the basis of cross-correlations on the radio star MWC349 (with  $S_{87\text{GHz}} = 950 \text{ mJy}$ ). This is in full agreement with the measured interferometer efficiency and should be accurate to 10%. The receiver passband shape was determined on 3C454.3 and its accuracy is better than 5% throughout the observing run.

Cleaned maps were obtained from the visibilities using the standard IRAM package. The maps were  $256 \times 256$  pixels in extent, with a pixel size of 0.4''. The synthesized beam, as determined by fitting a Gaussian to the dirty beam, is  $7.5'' \times 2.6''$ , oriented north-south (PA=180°). Due to the low declination of the galaxy, the uv plane is unequally sampled with a maximum spacing of 70 m in the north-south direction and of 250 m in the east-west. The corresponding east-west linear scale at the distance of the source, assuming  $D = 3.4 \text{ Mpc}$  (Sandage and Tammann 1975), is 42 pc. A continuum map was obtained by averaging visibilities over a bandwidth chosen to be free of line emission. In practice we used spectral channels with velocities 200  $\text{km s}^{-1}$  above and  $-200 \text{ km s}^{-1}$  below the galaxy's systemic velocity. For the effective 235 MHz bandwidth used to obtain continuum data, we derived a one  $\sigma$  point source sensitivity limit of 0.44 mJy/beam. The rms noise level in 5 MHz wide channel maps, as determined from the dirty maps after subtraction of the continuum, is 2 mJy/beam. This corresponds to an rms brightness temperature of 17 mK for the synthesized beam size and is consistent with a total on-source integration time of 15 hours and a mean system temperature of 150 K.

We have estimated the zero-spacing flux lacking in our maps. Taking into account that the shortest spacing measured by the interferometer is  $\sim 20 \text{ m}$ , we expect to filter out scales  $\sim 30''$ . Compared to the 30m data of **MP99**, only  $\sim 20\%$  of the single-dish flux in both SiO and H<sup>13</sup>CO<sup>+</sup> is missing within the primary beam. Therefore, our data offer an unbiased picture of the total SiO and H<sup>13</sup>CO<sup>+</sup> gas content in the nucleus of NGC 253.

We assume that the orientation of the NGC 253 disk is defined by the angle  $\text{PA}_{\text{disk}}=51^{\circ}$ , and inclination  $i=78.5^{\circ}$ . The orientation of the major axis of the stellar bar, along  $\text{PA}_{\text{bar}}=68^{\circ}$ , is used on purpose in some figures throughout the paper.

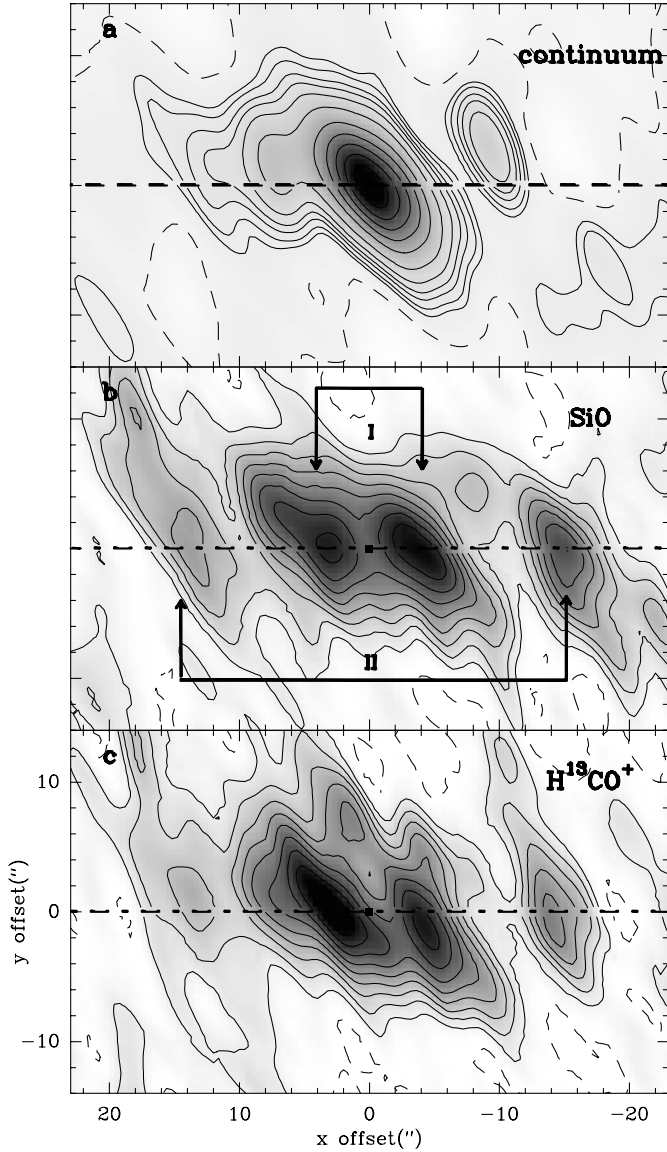


**Fig. 1. a:** Emission contours of the 3mm (86.7GHz) continuum source at the center of NGC 253.  $x$  and  $y$  are offsets (in arcsec) with respect to the dynamical center derived in this work, at  $\alpha_{J2000}=00^h 47^m 33.18^s$ ,  $\delta_{J2000}=-25^\circ 17' 17.2''$ ;  $x$  and  $y$  axes are parallel to the major and minor axes of the stellar bar, respectively ( $x$  runs parallel to  $PA_{bar}=68^\circ$ ). Contours are -1.5, 1.5, 2.5, 4, 5.5, 8 and 13 to  $64\text{mJybeam}^{-1}$  by steps of  $9\text{mJybeam}^{-1}$ .  $1\sigma$ -noise level is  $0.44\text{mJybeam}^{-1}$ . **b:** SiO( $v=0, J=2-1$ ) integrated intensity contours towards the center of NGC 253. Contours are -0.2, 0.2 to  $2.2\text{Jy.kms}^{-1}\text{beam}^{-1}$  by steps of  $0.25\text{Jy.kms}^{-1}\text{beam}^{-1}$ .  $1\sigma$ -noise level in the integrated intensity is  $0.07\text{Jy.kms}^{-1}\text{beam}^{-1}$ . Orientation as in Fig. 1a. **c:** same as **b** but for the  $J=1-0$  line of  $\text{H}^{13}\text{CO}^+$ , with same contours, noise level and orientation.

### 3. The interferometer maps

#### 3.1. The radio continuum emission

The 3mm continuum emission contours are plotted in Fig. 1a. Despite its compactness, this continuum source, with a peak flux of  $70\text{mJy/beam}$ , is resolved by our beam, with 80% of the

flux coming from the central source with a deconvolved size of  $\sim 8'' \times 4.3''$ , oriented along the disk major axis ( $PA \sim 50^\circ$ ). The integrated flux amounts to  $0.250 \pm 0.008\text{Jy}$ ; extrapolating fluxes at 6cm and 2cm (Turner & Ho 1985), we estimate that nonthermal and thermal free-free emission account each for one third of the observed 3mm continuum flux. The remaining third would come from emission by dust. Although our value for the integrated flux agrees within the errors with that measured at 85GHz by Carlstrom et al. (1990) ( $0.300 \pm 0.050\text{Jy}$ ), it is slightly lower than that derived by P96 at 98GHz ( $0.320 \pm 0.030\text{Jy}$ ).

The better sensitivity of our maps, compared with prior observations (Carlstrom et al. 1990; P96) reveals the presence of two previously undetected sources located along the bar major axis at offsets  $x=-10''$  and  $x=10''$ . These new sources appear marginally as extensions in the 1.3mm maps of Krügel et al. (1990). This suggests that they correspond mostly to dust emission. However the nature of these 3mm new sources is unknown. Comparison of our data with measurements at other wavelengths is not straightforward because of the missing flux in the images at the centimeter range and, on the other hand, owing to the lack of resolution of the existent maps at 1.3mm, 0.8mm and 0.45mm. Before high angular resolution observations at short millimeter and submillimeter wavelengths are obtained, little can be said on the nature of these new sources.

Contrary to P96, we see no extension of continuum emission to the southwest of the nucleus, interpreted as a signature of the giant outflow detected in X-rays. Continuum emission of the dust outflow has only been tentatively detected at 0.45mm by Alton et al. (1999), but it is absent in the 1.3mm and 0.8mm maps. We have extrapolated the flux measured at 0.45mm to 3mm and corrected for different resolutions, assuming an emissivity law of  $\sim \nu^2$ . We predict a 3mm counterpart of  $0.1\text{mJy/beam}$  for the dust outflow in NGC 253, well beyond the noise level in our map ( $0.44\text{mJy/beam}$ ) and a factor of  $\sim 200$  weaker than the 3mm extensions of P96, that reveal as spurious.

#### 3.2. The SiO and $\text{H}^{13}\text{CO}^+$ emission

Fig. 2 shows the velocity-channel maps obtained in the ( $v=0, J=2-1$ ) line of SiO at the centre of NGC 253; Fig. 3 shows the same but in the ( $J=1-0$ ) line of  $\text{H}^{13}\text{CO}^+$ . Gas emission is unevenly distributed in the velocity range [ $120-353\text{kms}^{-1}$ ]. This arises from a circumnuclear disk (CND) extending over  $600\text{pc} \times 150\text{pc}$ . The disk, seen at high inclination ( $i=78.5^\circ$ ), is radially resolved and displays an overall rotating pattern.

Although the dominant trend is circular rotation, we also find emission at highly non-circular velocities in both tracers. The emission is patchy in both lines, most noticeably, the SiO and  $\text{H}^{13}\text{CO}^+$  clumps show no one-to-one correspondence over the map: as discussed below (Sect. 7), the  $T_{mb}(\text{SiO})/T_{mb}(\text{H}^{13}\text{CO}^+)$  ratio has a wide range of variation in the nucleus of NGC 253 (i.e.  $T_{mb}(\text{SiO})/T_{mb}(\text{H}^{13}\text{CO}^+) \sim 0.5-8$ ).

The CND also shows structure along the apparent minor axis. The velocity-integrated intensity maps of SiO ( $I_{SiO}$ ) and  $\text{H}^{13}\text{CO}^+$  ( $I_{H^{13}CO^+}$ ), shown in Figs. 1b-c, illustrate the CND substructure. Spatial coordinates are arcsecond offsets along

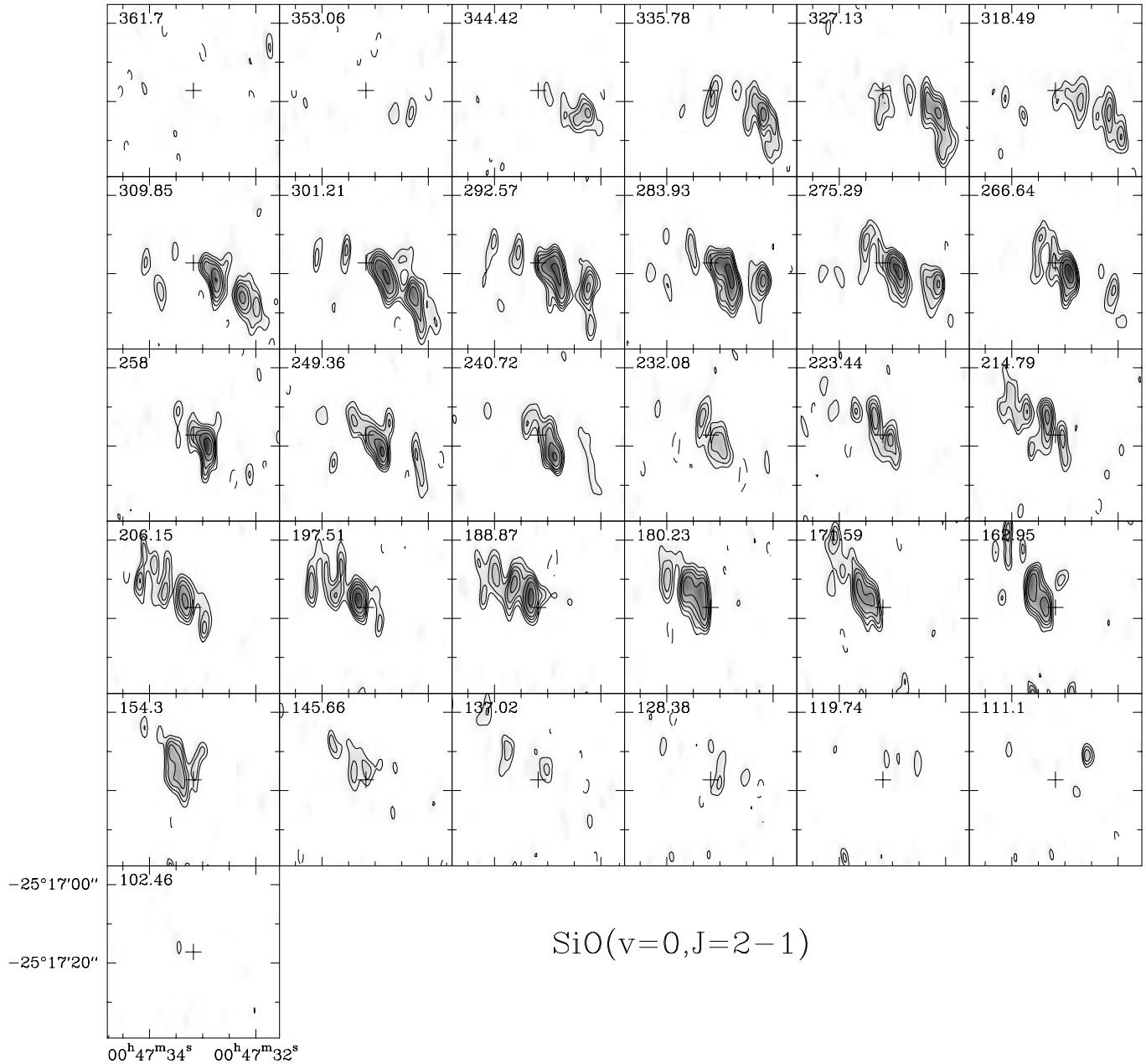


**Fig. 2.** SiO ( $v=0, J=2-1$ ) velocity-channel maps observed with the IRAM interferometer of Plateau de Bure with a resolution (HPBW) of  $7.5'' \times 2.6''$  ( $PA=180^\circ$ ). Absolute coordinates are 2000.0 (the derived dynamical center is indicated by the cross at  $\alpha_{J2000}=00^h47^m33.18^s$ ,  $\delta_{J2000}=-25^\circ17'17.2''$ ). Velocity-channels range from  $v=361.5\text{km s}^{-1}$  to  $v=93.8\text{km s}^{-1}$  by steps of  $-8.6\text{km s}^{-1}$ . Contour levels are -6, 6, 8, 10, 12, 15, 19 and  $23\text{mJy beam}^{-1}$ .  $1\sigma$ -noise level is  $2\text{mJy beam}^{-1}$ . Axes are  $(\alpha, \delta)$ .

the principal axes of the near infrared (NIR) stellar bar (Scoville et al. 1985). The bar major axis (denoted  $x$ ) is at  $PA=68^\circ$ , with  $x>0$  eastwards (the bar minor axis, denoted  $y$ , lies along  $PA=158^\circ$ , with  $y>0$  northwards). Fig. 1b shows that the SiO emission mostly comes from two-nested rings centered at  $(0,0)$  and roughly oriented parallel to the  $x$  axis. A similar morphological description applies to  $\text{H}^{13}\text{CO}^+$  map (Fig. 1c), although here the inner ring orientation deviates significantly from the bar major axis.

The inner ring (**I**), of average diameter  $D_I \sim 8''$  (120pc), contains 60-70% of the total flux in the two lines and it corresponds to the region of the massive starburst in NGC 253 seen in different tracers. The emission of the outer ring (**II**), of average diameter  $D_{II} \sim 24''$  (360pc), contains 20-30% of the total flux. The two nested rings share as common center the peak of the 3mm continuum source. Emission in **I** is detected within a large velocity range for the two edges of the ring ( $\sim 120\text{km s}^{-1}$ ). This spread is symmetrical with respect to the continuum source locus (a similar symmetry is seen to hold for **II**). We therefore identify

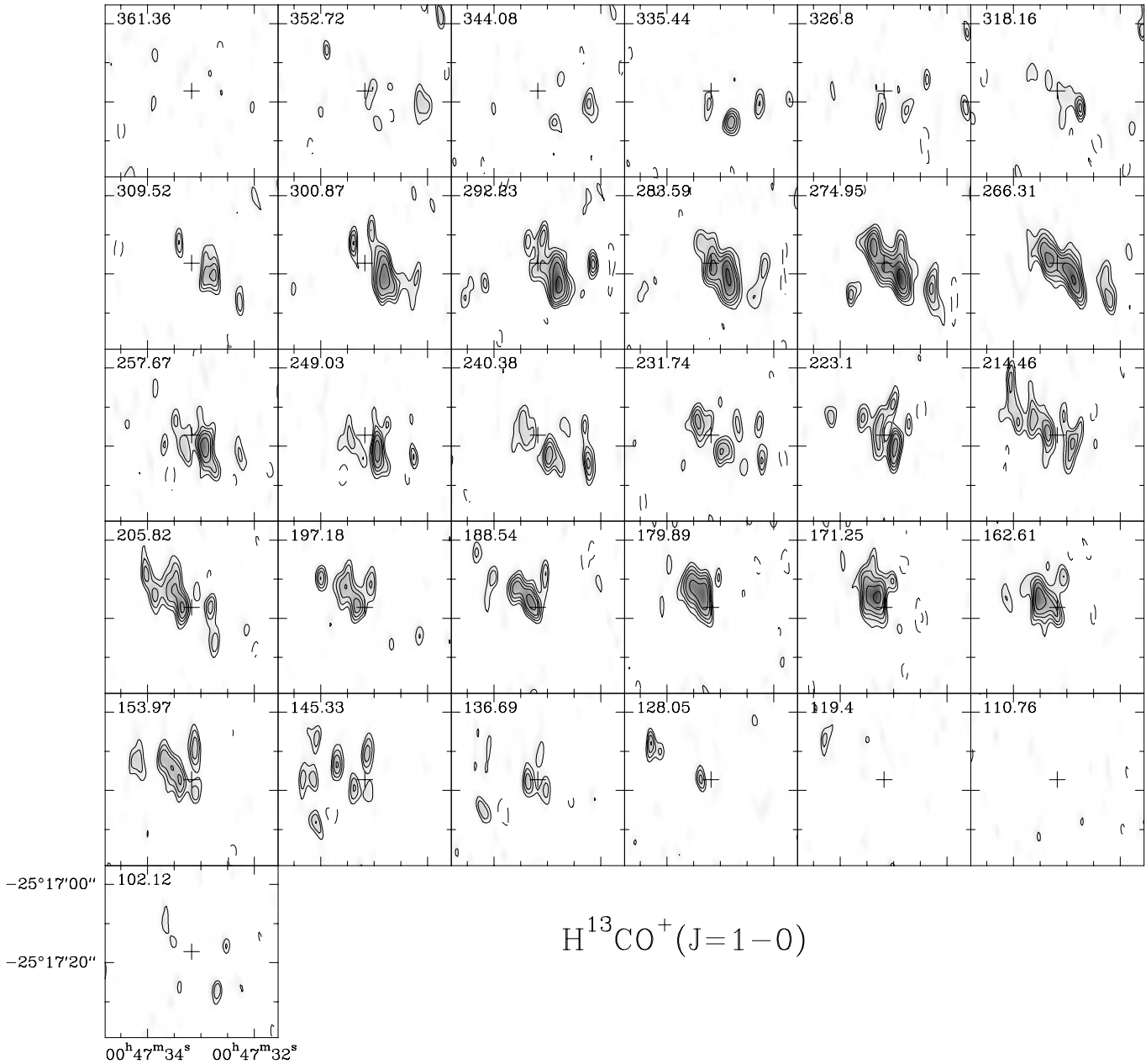


**Fig. 3.** Same as Fig. 2 but for the  $\text{J}=1-0$  transition of  $\text{H}^{13}\text{CO}^+$  with the same levels, velocity spacing and axes orientation.

it as the dynamical center of NGC 253 ( $\alpha_{J2000}=00^{\text{h}}47^{\text{m}}33.18^{\text{s}}$  and  $\delta_{J2000}=-25^{\circ}17'17.2''$ ). This position coincides, within the errors, with the dynamical center determined using optical (Watson et al. 1996), infrared (Sams et al. 1994, Boker et al. 1998) and radio data (Turner & Ho 1985).

Although most of the emission arises from the double ringed source (**I-II**), we have also detected gas outside the x axis: the CNB structure along the minor axis is partly resolved. Although part of the emission can be accounted by the gas distribution in the CNB disk seen in projection (NGC 253 is not fully edge-on), at places, the emission lies far away from the NIR bar major axis, and most noticeably, this corresponds to gas clouds showing highly non-circular motions and a high relative abundance

of SiO ( $T_{mb}(\text{SiO})/T_{mb}(\text{H}^{13}\text{CO}^+)=3-5$ ). In particular, the SiO emission channels of Fig. 2 in the range  $[284-335\text{km s}^{-1}]$  show receding gas ( $v-v_{sys}=80\text{km s}^{-1}$ ; where  $v_{sys}=235\text{km s}^{-1}$ ) in the SE quadrant, where *it should be* approaching. As will be discussed below, the origin of this *anomalous* component is related with the giant outflow detected in X-ray and optical emission lines. This does not have the same origin as **I-II**. However, there is a  $\text{H}^{13}\text{CO}^+$  clump at  $(x,y)\sim(1,8)$  which shows no SiO counterpart. Contrary to the anomalous component, this might correspond to disk gas seen in projection. This clump has a low ratio  $T_{mb}(\text{SiO})/T_{mb}(\text{H}^{13}\text{CO}^+)\sim 0.3$ , and most important, it lies close to the minor axis of the galaxy appearing at velocities close to  $v_{sys}$ .

#### 4. The CNB structure

To study the CNB structure we have obtained the peak brightness flux distributions in the two lines ( $B^{peak}(x,y)=\max[T_{mb}]_v(x,y)$ ). This allows us to filter out the lower spatial frequencies enhancing the most intense features in the maps. Then we deprojected  $B^{peak}$  onto the galaxy plane, in order to get a sharp picture of the CNB, viewed face-on. The result is shown in Figs. 4a-b. The peaks of emission of ring **I** are rather aligned with the major axis of the disk, tilted  $20^\circ$  clockwise with respect to the bar major axis. The tilt is more pronounced for  $\text{H}^{13}\text{CO}^+$  (Fig. 4a). On the contrary, the peaks of emission of ring **II** open out, go across the line of the bar major axis and delineate a spiral-like arc. The face-on picture of the CNB of Fig. 4a consists of a gaseous spiral-like ridge (**II**) ending up in an unresolved ring **I** viewed edge-on and aligned with the major axis of the disk.

Interferometer observations by Canzian et al. (1988) have shown that the bulk of molecular gas in the CNB, traced by the 1–0 line of  $^{12}\text{CO}$ , is distributed in a bar-like source, oriented in the direction of the NIR bar. The recent  $^{13}\text{CO}$  map of Hüttemeister and Aalto (1998) confirms this view. In contrast, the distribution of dense gas ( $n(\text{H}_2) > 10^{5-6} \text{cm}^{-3}$ ) is similar to the  $B^{peak}$  maps of SiO and  $\text{H}^{13}\text{CO}^+$ . The CN(1–0) and HNC(1–0) maps of Hüttemeister and Aalto (1998) show a centrally condensed inner disk of diameter  $\sim 8''$ , oriented along  $\text{PA}=45^\circ$ – $50^\circ$ , while the outer disk tilts farther towards  $\text{PA}=70^\circ$ , delineating a spiral-like arc that goes across the major axis of the stellar bar. The same applies for the HCN(1–0) map of Paglione et al. (1995): the inner disk is better aligned with the disk major axis  $\text{PA}=45^\circ$ , whereas the outer ring tilts progressively towards  $\text{PA}=70^\circ$ .

There is little doubt that NGC 253 contains a stellar bar oriented along  $\text{PA}=68^\circ$  and extended  $300''$  on the sky, which sets a lower limit for its corotation radius at  $R_{COR}=150''$  (Scoville et al. 1985). P96 first explained the distribution of the CS(2–1) emission in terms of a bar potential. However the parameters of the bar were chosen arbitrarily: the bar corotation is placed at  $40''$ , a factor of  $\sim 4$  too short, compared with the estimated bar semi-major axis ( $\sim 150''$ ). The NIR image of the bar is distorted by dust extinction. There are two dust lane ridges offset with respect to the bar major axis. Assuming that the NW is the near side of NGC 253 (De Vaucouleurs 1958), the two offset dust lanes inside the bar represent a trailing spiral wave. This pattern is an indication of the existence of two Inner Lindblad Resonances (outer=oILR and inner=iILR; see Athanassoula (1992)). The morphology of the gas response in the presence of two ILRs has been analysed by several authors (see Buta and Combes 1996 and references therein). Owing to dissipation by cloud-cloud collisions, the gas cannot follow the periodic orbits of the stars in a bar ( $x_1$ =parallel, between corotation and oILR or  $x_2$ : antiparallel, between the oILR and the iILR). The gas response always leads the stellar orbits, giving a trailing spiral inside the bar corotation that goes across the oILR. It is tempting to identify the spiral-like **II** as the oILR. The gas compression along the spiral ridges should be best traced, as observed,

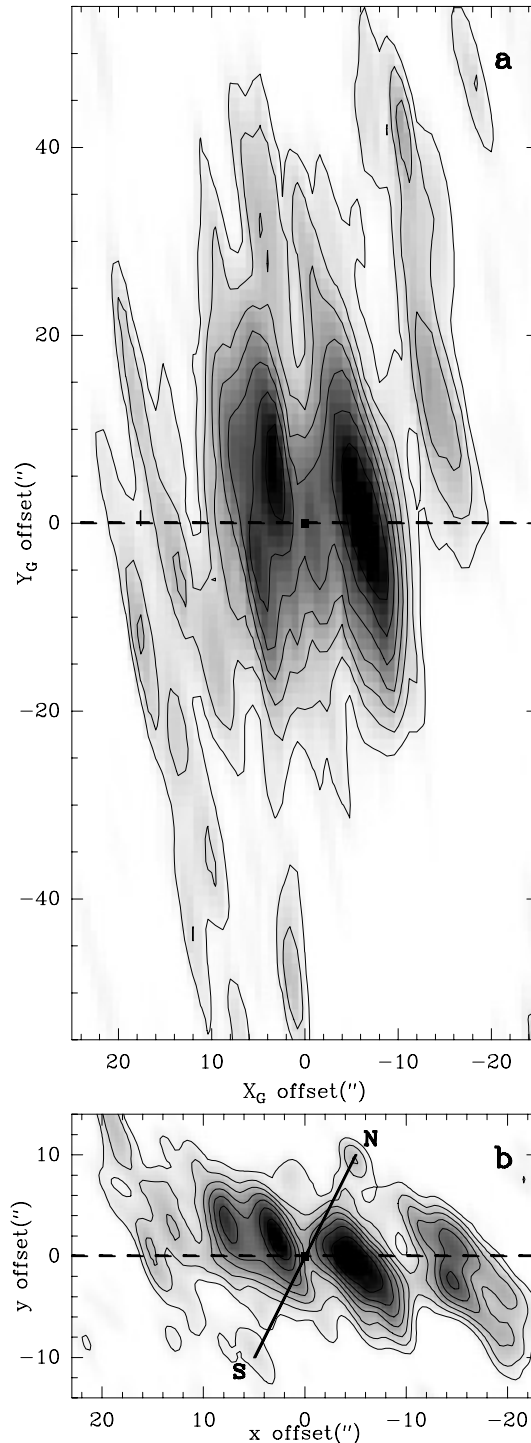


**Fig. 4.** **a:**  $\text{H}^{13}\text{CO}^+(1-0)$  peak-brightness flux contours in the CNB of NGC 253, deprojected onto the galaxy plane ( $(X_G, Y_G)$ ; where  $X_G$  runs parallel to the major axis of the disk along  $\text{PA}_{disk}=51^\circ$ ), displayed from 7 to 19 mJy/beam by steps of 2 mJy/beam. The inner region is a nearly edge-on ring encircling the starburst, whereas the outer region opens up towards larger PAs, delineating a spiral-like arc. **b:** SiO( $v=0, J=2-1$ ) peak-brightness temperature contours in the CNB of the galaxy, as seen in the plane of the sky in  $(x, y)$  coordinates as defined in text. Same contours as **a**. The thick line high-lights the orientation of the N and S filaments.

by the higher density tracers of molecular gas. In contrast, the nuclear spiral across the oILR is washed out in the  $^{13}\text{CO}$  and  $^{12}\text{CO}$  maps tracing the low or moderately dense molecular gas ( $n(\text{H}_2)=10^{3-4}\text{cm}^{-3}$ ).

Moreover, the proposed resonance loci of the bar naturally explain the double-ringed appearance of NGC 253 (Figs. 1bc), and how the nuclear starburst might have been onset. When a barred galaxy has two ILRs, as NGC 253, gas tends to accumulate at the iILR, as a consequence of secular evolution. The engine behind the radial inflow of gas is double. Gravity and viscous torques cooperate in bringing the gas closer to the nucleus. Gravity torques act on the gaseous spiral expected to form between the iILR and oILR. The spiral is a superposition of leading and trailing waves. The leading wave dominates at the crossing of the iILR, whereas the trailing wave develops at the crossing of the oILR (Buta and Combes 1996). The gravity torques change their sign at the crossing of the resonances, and also when we move from the trailing to the leading spiral (Combes 1994a, 1994b). The net result would be the formation of two pseudo-rings at the iILR and the oILR, with similar time-scales. However, viscous torques being always negative, may break this symmetry making the gas migrate towards the iILR in a few dynamical times ( $\sim 10^{7-8}$  years) and therefore progressively depopulate the oILR. The oILR may end up as a trailing spiral-like pseudo-ring (ring **II** in NGC 253), whereas the leading spiral vanishes into the inner ring (similar to ring **I**).

It seems that the morphology of the  $\text{SiO}/\text{H}^{13}\text{CO}^+$  maps and how they compare to other molecular gas tracers can be explained by gas accumulation at the ILRs of the bar in NGC 253. Arnaboldi et al. 1995, used the  $\text{H}\alpha$  major axis kinematics to make an independent estimation of the bar resonances loci. Within the epicyclic approximation, they identified two ILRs in the nucleus of NGC 253. Assuming a lower limit for the bar corotation,  $R_{\text{cor}}=3.9\text{kpc}$ , they derived an oILR at  $300\text{pc}$  ( $20''$ ) and the iILR near the center, in agreement with what is proposed in this work. Studying the gas kinematics in the  $\text{SiO}/\text{H}^{13}\text{CO}^+$  CND will allow to test the location of the principal resonances and understand the relation between the starburst and the bar.

## 5. Kinematics of the CND

There is a wealth of published work on the dynamics of the ISM in the nucleus of NGC 253. The determination of a rotation curve ( $v_{\text{rot}}$ ) for the nucleus of NGC 253 has been very controversial because of extinction (Ulrich 1978). The high-sensitivity  $\text{H}\alpha$  data of Arnaboldi et al. 1995, already showed a velocity gradient more symmetrical and steeper than seen in previous optical surveys.

Figs. 5a-b show the  $\text{SiO}$  and  $\text{H}^{13}\text{CO}^+$  position-velocity diagrams taken along the kinematical major axis of the disk of NGC 253 ( $x'$  axis). In view of the high inclination of NGC 253, the terminal velocity method would be well suited to derive  $v_{\text{rot}}$  from the major axis kinematics. However the patchiness of the  $\text{SiO}/\text{H}^{13}\text{CO}^+$  emission makes any fit uncertain. There are strong oscillations of the terminal velocities as a function of radius, revealing an uneven gas distribution and/or the presence of

non-circular motions. As a zero-order approach we will adopt  $v_{\text{rot}}$  derived by Canzian et al (1988) from CO. This species is the best tracer of molecular gas at a large-scale, from densities as low as  $n(\text{H}_2)\sim 10^3\text{cm}^{-3}$ , and although non-circular motions should also affect the observed kinematics, the estimated  $v_{\text{rot}}$  would be closer to the axisymmetric value.

The centroid of  $\text{SiO}/\text{H}^{13}\text{CO}^+$  emission in the major axis p-v plots follows closely  $v_{\text{rot}}(\text{CO})$ , but most noticeably, the emission shows a large velocity spread around ( $\Delta_v=100\text{-}120\text{kms}^{-1}$ ; see Figs. 5a-b). The observed linewidths could be partly due to the smearing of  $v_{\text{rot}}$  within our beam. Assuming  $i=78.5^\circ$ , we expect to get emission from clouds at  $y_{\text{depr}}=\pm 9\text{-}10''$  ( $y_{\text{depr}}$  is the deprojected distance from which emission is seen by our beam along  $y'$ ). Along the major axis we get emission from  $x'=\pm 1.6''$ .  $v_{\text{rot}}(\text{CO})$  follows a rigid body law with a velocity gradient of  $6\text{kms}^{-1}''$ , from which we derive an upper limit for the total velocity broadening of  $\sim 60\text{kms}^{-1}$  within our beam, i.e., a factor of  $\sim 2$  lower than the observed velocity spread.

The existence of a large velocity dispersion in the CND gas cannot be excluded (we would need  $\sigma_v\sim 40\text{-}50\text{kms}^{-1}$  to explain the observed linewidths). However, an explanation of the  $\text{SiO}/\text{H}^{13}\text{CO}^+$  linewidths in terms of unresolved non-circular motions is more plausible as it is supported by additional observational evidence.

Firstly, a part of the emission is detected at velocities that cannot be accounted by *any* circular rotation law. These regions in the major-axis p-v plots correspond to the ( $x',v$ )-quadrants ( $x'>0, v>v_{\text{sys}}$ ) and ( $x'<0, v<v_{\text{sys}}$ ).  $\text{SiO}/\text{H}^{13}\text{CO}^+$  gas emission fills unevenly a romboïd-like parallelogram in Figs. 5a-b. The symmetry of the above pattern is remarkable and it reminds of the signature of bar-driven elliptical orbits developed inside the ILR domain (Binney et al. 1991; García-Burillo and Guélin 1995, Fux 1998, García-Burillo et al. 1999). The parallelogram boundary would correspond to the inner non-selfintersecting  $x_1$  orbit (called the *cusped* orbit). Inside, gas clouds lie along precessing  $x_2$  orbits whose envelope delineate a spiral across the oILR; these orbits are highly elliptical and produce the observed non-circular motions. The velocity gradient is reversed for a  $\text{SiO}$  component in the major axis p-v plot between  $x'=-4''$  and  $x'=4''$ . The latter was also reported by **P96** in the CS p-v plot and by Ananthamaraiah and Goss(1996) using recombination-line data. *Apparent* counter-rotation can also be explained by bar orbits (see Fig. 8 of García-Burillo and Guélin 1995). The  $\text{SiO}$  minor axis position-velocity diagram, displayed in Fig. 6a, suggests also that gas distribution in the nucleus deviates from axisymmetry. The cut along the minor axis is markedly asymmetrical: the centroid of redshifted gas lies  $1''\text{-}2''$  above the major axis locus, whereas blue-shifted gas lies  $1''\text{-}2''$  below.

Ananthamaraiah and Goss(1996) reported the existence of a complex kinematic subsystem in the inner  $150\text{pc}$  of NGC 253, using recombination-line data. The nucleus would host three gaseous disks; among the anomalous components, one exhibits rotation in a plane perpendicular to the galactic disk, and the inner disk is *apparently* counter-rotating. These components are introduced to explain deviations from circular motions similar to what is shown in our data. On the basis of this somewhat *ad hoc*

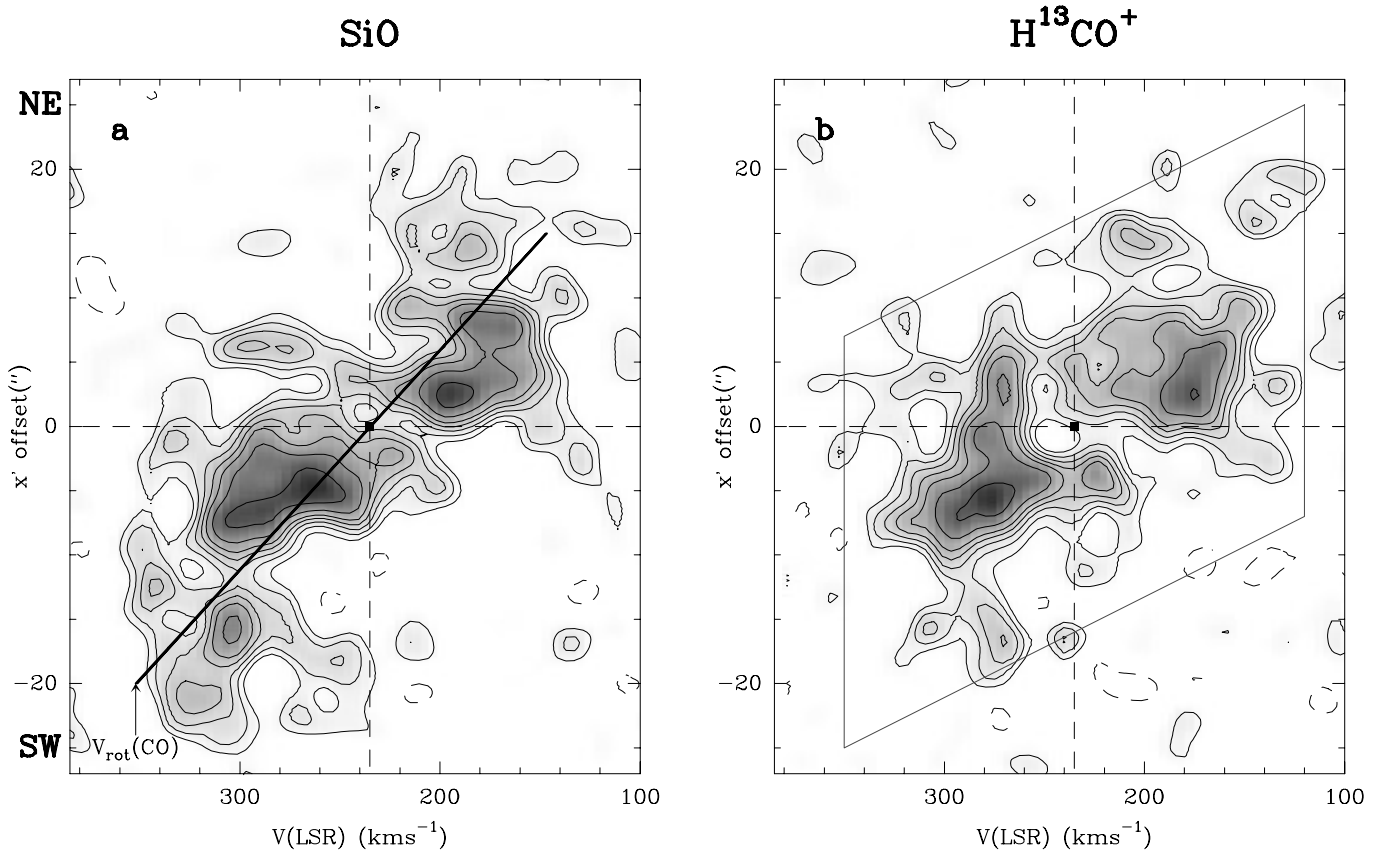


**Fig. 5a and b.** The major axis (along  $PA=51^\circ$ ) position-velocity diagrams taken at the center of NGC 253 in the SiO( $v=0, J=2-1$ ) **a** and  $H^{13}CO^+$  **b** lines.  $x'$  offsets along major axis ( $PA=51^\circ$ ) are referred to the dynamical center derived in this work:  $\alpha_{J2000}=00^h 47^m 33.18^s$  and  $\delta_{J2000}=-25^\circ 17' 17.2''$ .  $v_{sys}(LSR)$  is taken at  $235\text{km s}^{-1}$ . Contours are  $-0.004, 0.004, 0.006, 0.008, 0.010, 0.012, 0.015, 0.019$  and  $0.023\text{Jy beam}^{-1}$ . Our effective resolution along the major axis is  $\Delta x' \times \Delta v = 3.2'' \times 8.6\text{km s}^{-1}$ . The rotation curve derived from CO ( $v_{rot}(CO)$ ) is superposed to Fig. 5a. The romboid-like parallelogram delimits the p-v space occupied by bar-driven orbits inside the ILR domain (see text).

decomposition, the authors find evidence of a past merger involving a small mass companion. However, the merger hypothesis is unable to explain the undisturbed morphology and kinematics of the outer disk (Olson and Kwan, 1990). The distorted kinematics of the NGC 253 nucleus, including the existence of strong non-circular motions detected also in the recombination-line data, are more readily explained in terms of a bar-driven gas flow.

## 6. A molecular gas counterpart of the NGC 253 nuclear outflow

In the previous section we have argued that the bulk of the SiO/ $H^{13}CO^+$  emission in the CNB fits within the bar-driven gas flow scenario. However, we reported in Sect. 3 the detection of an anomalous component which might be far from the CNB plane. The off-axis gas, mostly detected in the SiO line ( $T_{mb}(\text{SiO})/T_{mb}(H^{13}CO^+)=3-5$ ), is best seen towards the south (*down the plane* of the CNB). The southern SiO plume starts at the base of the starburst ring **I** and it reaches a *height* of  $\delta y=10''$  (measured from the major axis of the bar; see Fig. 4b). The gas shows also strong deviations from circular motion ( $\Delta v \sim 100-150\text{km s}^{-1}$ ) and its emission spreads over  $\sim 200\text{km s}^{-1}$  (see

Fig. 6b). There is a much weaker and point-like counterpart of the southern SiO-plume towards the North. The northern gas shows also strong noncircular motions ( $\Delta v \sim 150\text{km s}^{-1}$ ) but it is here characterized by a narrow profile ( $\sim 17\text{km s}^{-1}$ ). SiO spectra towards these positions are displayed in Fig. 7. The Northern and Southern plumes (hereafter called N and S) can be connected by a line that goes across the dynamical center; the N-S line has a  $PA=131^\circ$  measured from North (see Fig. 4b). This orientation places the anomalous component close to the galaxy minor axis ( $PA=141^\circ$ ) where no contribution from rotation curve in the radial velocity gradient is expected. Moreover it is hard to explain non-circular motions of  $\Delta v \sim 100-150\text{km s}^{-1}$  due to bar forcing in the plane of the galaxy.

There is compelling evidence for the existence of a giant outflow of gas in the nucleus of NGC 253. Demoulin and Burbidge(1970) and Ulrich (1978) were the first to report the presence of an ionized gas outflow, based on the analysis of gas kinematics derived from  $H\alpha$  spectroscopy. Soft X-ray emission from the giant outflow was later discovered by Fabbiano and Trinchieri (1984). The X-ray nebula is more extended to the southern part of the galaxy minor axis and was interpreted as thermal emission of gas heated by fast shocks, driven by a bipolar wind coming from the starburst. Further support for

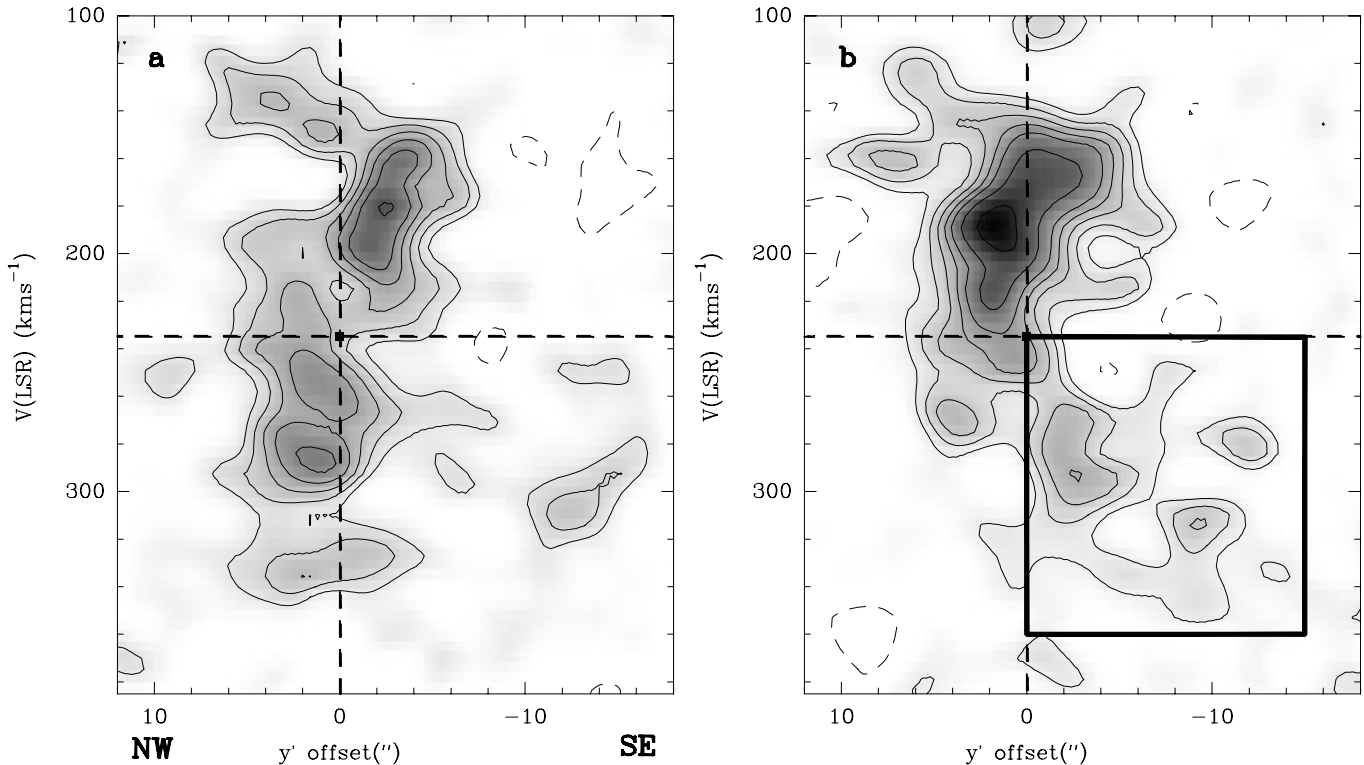


**Fig. 6.** **a** SiO strip along the minor axis of the galaxy (PA=141°) with same contours as Fig. 5. The effective resolution is  $\Delta y' \times \Delta v = 4'' \times 8.6 \text{ km s}^{-1}$ . We also display in **b** the SiO position-velocity diagram parallel to the minor axis, but taken at  $x=4''$ , showing the presence of gas emission at highly non-circular motions (inside the high-lighted region).

this scenario is provided by the distribution of ionized gas in the outflow, which adopts the form of filaments that border the X-ray nebula (McCarthy et al. 1987). Furthermore, Schulz and Wegner (1992) detected line-splitting in NII, SII and HII, consistent with the ionized gas lying across the conical working surface of the X-ray nebula. The gas entrainment by the hot wind may cause shock-heating and subsequent emission. The observed line-splitting, together with the inferred expansion velocities ( $\sim 390 \text{ km s}^{-1}$ ), are the main arguments supporting the shock-heating scenario.

Very recently, Alton et al. 1999 have reported the tentative detection of submillimeter emission at  $450 \mu$  coming from one filament associated with the S outflow. The location of the S filament agrees reasonably well with the one detected in SiO/H $^{13}\text{CO}^+$  (see above and Fig. 4b). The dust mass contained in the filaments, which partly depends on the dust temperature, cannot be easily estimated from the detection at just one wavelength. No counterpart of the dust outflow is seen neither at 1mm nor at 3mm, as expected from the flux detected at  $450 \mu$  (see discussion of Sect. 3.1; see also Krügel et al, 1990). However we can try to estimate the dust column density towards the S filament from the flux reported by Alton et al. 1999, corrected to our beam. We assume a dust emissivity spectral index of  $\beta=2$ , the emissivity law is taken from Chini et al. (1997), and adopt a dust temperature in the range  $T_{\text{dust}}=13\text{K}-37\text{K}$  (similar to the model that fits the M82 dust outflow: Alton et al. 1999). We calculate a range of  $N_{\text{dust}} \sim 0.6-4 \times 10^4 M_{\odot}$

towards the S filament, within our beam. If  $M_{\text{gas}}/M_{\text{dust}}=100$ , this results implies  $N(\text{H}_2) \sim 0.6-4 \times 10^6 M_{\odot}/\text{beam}$ . As discussed in Sect. 7, we can estimate  $N(\text{H}_2)$  in the S filament where H $^{13}\text{CO}^+$  is detected, using  $N(\text{H}^{13}\text{CO}^+)$  derived from a Large Velocity Gradient (LVG) transfer model and assuming  $X(\text{H}^{13}\text{CO}^+)=10^{-10}$  (see discussion of Sect. 7 for details). We calculate  $N(\text{H}_2) \sim 3.5 \times 10^6 M_{\odot}/\text{beam}$  ( $4.7 \times 10^{22} \text{ cm}^{-2}$ ), roughly in agreement with the value estimated from the dust emissivity. Therefore no contradiction exists between the failed detection of the S outflow in the continuum and the successful detection of the outflow in the two lines of SiO and H $^{13}\text{CO}^+$ .

If the molecular CND is locally disrupted and it is entrained by the hot wind out of the plane, we can expect that the geometries for the working surfaces of molecular and ionized gas should be alike. The parameters of Schulz and Wegner's model are an expansion velocity of  $390 \text{ km s}^{-1}$  for the conical outflow coming out of the plane, and a half-opening angle of  $25^\circ$ . Projection effects along the line of sight would make appear two velocities at each position of the outflow (N or S). The emission from the S(N) filament should appear either at  $v_{\text{rad}}=-10 \text{ km s}^{-1}$  ( $120 \text{ km s}^{-1}$ ) or at  $v_{\text{rad}}=300 \text{ km s}^{-1}$  ( $440 \text{ km s}^{-1}$ ). The velocities observed in the SiO lines for the N ( $v_{\text{rad}}=100 \text{ km s}^{-1}$ ) and S filaments ( $300 \text{ km s}^{-1}$ ) confirm the predictions of Schulz and Wegner's model, originally intended to fit the observed line-splitting in the optical lines. Turner (1985) was the first to report the existence of a molecular gas ejection event in the NGC 253 nucleus. However, the location of the OH plume hardly fits the morphol-

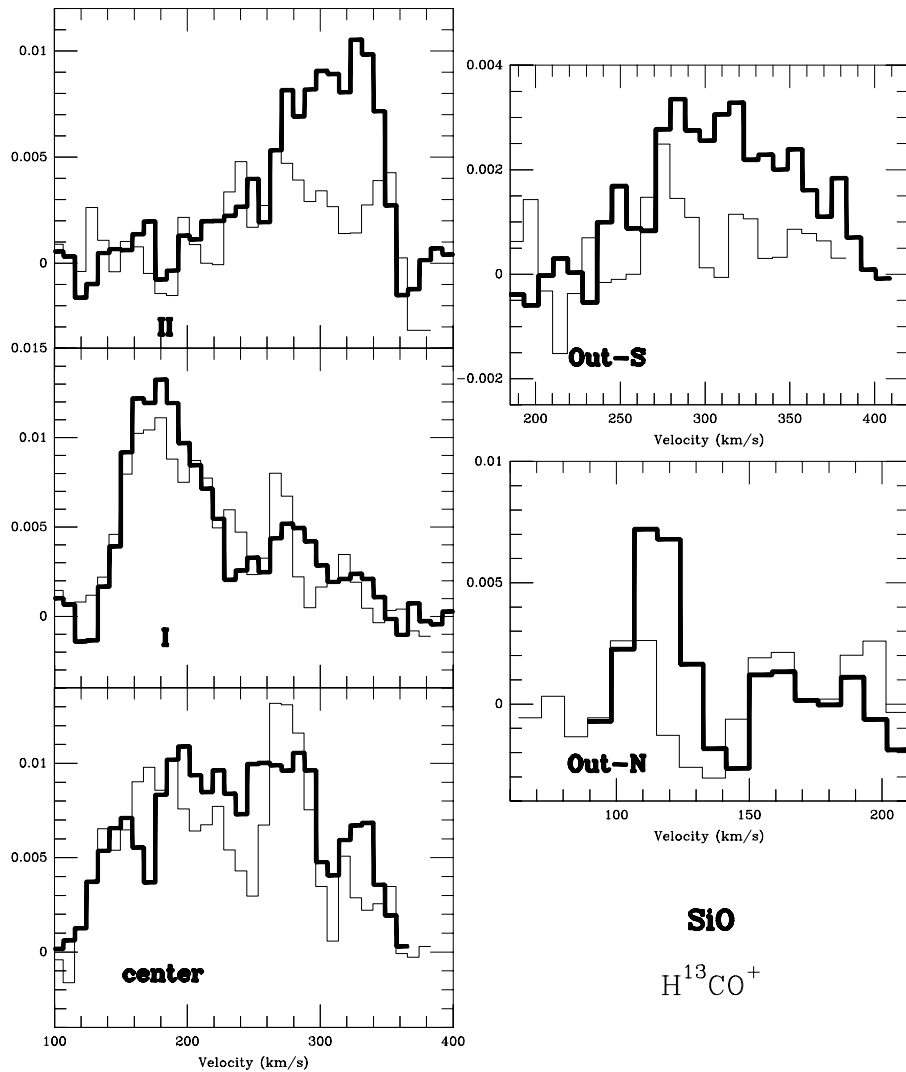


**Fig. 7.** We compare the SiO ( $v=0, J=2-1$ ) (thick line) and  $H^{13}CO^+$  (thin line) spectra at several positions:  $(x,y)=(0'',0'')$  (**left bottom**) in the dynamical center,  $(x,y)=(3.2'',3.2'')$  (**left middle**) in region **I**,  $(x,y)=(-17.6'',1.6'')$  (**left top**) in region **II**,  $(x,y)=(3'',-8'')$  (**right top**) in the southern outflow and  $(x,y)=(-5'',8'')$  (**right bottom**) in the northern outflow; the spectra illustrate the large variations of the  $T_{mb}(SiO)/T_{mb}(H^{13}CO^+)$  ratio in the **CND**. Y axis scale is in  $Jy/beam$ .

ogy and kinematics of the ionized or molecular outflow: the OH gas is ejected from the nucleus towards the NE quadrant (along  $PA=6^\circ$ ) and it reaches  $\sim 1kpc$  height (see Fig. 11 of Turner 1985 for details).

We conclude that the distribution and kinematics of the off-axis component detected in our maps are easily accounted for if we suppose that the emission comes from molecular gas in an outflow leaving the nucleus, out of the galaxy plane. Furthermore, an estimate of the molecular gas mass involved in the outflow seems to be consistent with the dust emissivity of the filaments.

### 7. The $T_{mb}(SiO)/T_{mb}(H^{13}CO^+)$ and $N(SiO)/N(H^{13}CO^+)$ ratios

The line temperature ratio  $R_{T_{mb}}=T_{mb}(SiO)/T_{mb}(H^{13}CO^+)$  shows large variations (0.5–8) in the nucleus of NGC 253; these variations however show a systematic trend. For the sake of simplicity, we first examine the ratio of velocity-integrated emission  $R_I=I(SiO)/I(H^{13}CO^+)$  averaged across those regions where  $R_I$  shows a characteristic value. We have chosen as cases of study

the dynamical center, regions **I–II** and the outflow components (N–S). Table 1 shows the mean values of  $R_I$  and its range of variation; Fig. 7 shows representative spectra for the regions studied. We see a clear trend in the ratios, which increase as one moves away from the vicinity of the starburst. The average ratios are  $R_I \sim 1.0$ , for the center,  $R_I \sim 1.1$  for the starburst ring **I**,  $R_I \sim 3$  for the outer region **II** and  $R_I \sim 2$  for the outflow. We will analyse the range of variation of  $R_{T_{mb}}$  for each region defined above, and derive the column density ratios  $N(SiO)/N(H^{13}CO^+)$  via a Large Velocity Gradient (LVG) scheme. Our objective is to study the range of physical parameters and chemical abundances of SiO clouds in the **CND**.

LVG solutions depend on three parameters: the density ( $n(H_2)$ ), the kinetic temperature ( $T_K$ ) and the abundance of the species. The kinetic temperature of molecular gas in the center of NGC 253 has been derived by several authors using multi-transition studies in  $^{12}CO$  and its isotopes ( $^{13}CO$  and  $C^{18}O$ ), CS and HCN; all indicate an average value of  $T_k > 50K$ . We have adopted  $T_k=50K$  as representative for the SiO clouds and taken  $n(H_2)$  from the fit to the ratios  $R_{32}=I(SiO(3-2))/I(SiO(2-$

**Table 1.** Table 1 fully explores the dependence of  $N(\text{SiO})/N(\text{H}^{13}\text{CO}^+)$  and  $X(\text{SiO})$  on  $\eta_{fill}$ ; the filling factor is varied within its whole range (0.005–1) and the results are displayed for the different regions of the nucleus where distinct values of  $R_I$  are measured. See text for details.

$n(\text{H}_2)=5 \times 10^5$ , $T_k=50$ K, $X(\text{H}^{13}\text{CO}^+)=10^{-10}$				
REGION	$R_I=T(\text{SiO})/T(\text{H}^{13}\text{CO}^+)$	$\eta_{fill}$	$N(\text{SiO})/N(\text{H}^{13}\text{CO}^+)$	$X(\text{SiO})$
Centre	1.0±0.2	1	1.1	$1.1 \times 10^{-10}$
		0.005	1.3	$1.3 \times 10^{-10}$
I	1.1±0.1	1	1.5	$1.5 \times 10^{-10}$
		0.005	2.0	$2.0 \times 10^{-10}$
II	3.0±1	1	5.0	$5.0 \times 10^{-10}$
		0.005	15.0	$1.5 \times 10^{-9}$
Out-S	2.0±1	1	3	$3 \times 10^{-10}$
		0.005	5	$5 \times 10^{-10}$
Out-N	2	1	3	$3 \times 10^{-10}$
		0.005	5	$5 \times 10^{-10}$

1)) and  $R_{54}=I(\text{SiO}(5-4))/I(\text{SiO}(3-2))$  derived by **MP99**, using single-dish 30m spectra. **MP99** found little evidence of a density decrease for the SiO clouds, at least within the inner  $r \sim 20''$  of the nucleus. They derived an average  $n(\text{H}_2)=5 \times 10^5$  assuming a common filling factor for the three lines. We will take this estimation as representative for SiO and  $\text{H}^{13}\text{CO}^+$  in our model. Note that although there might be a hotter component in the nucleus ( $T_k \sim 100$ K; see Mauersberger et al. 1990), we must stress that  $n(\text{H}_2)$  inferred from the SiO line ratios depend weakly on the adopted kinetic temperature if  $T_k > 50$ K.

Fig. 8 displays the range of LVG solutions that fit  $R_{32}$  and  $R_{54}$  within the errors. The assumed density  $n(\text{H}_2)=5 \times 10^5$  fits satisfactorily  $R_{32}$  and  $R_{54}$ , for a large interval of  $N(\text{SiO})/\Delta_v$ . Trying to delimit the LVG solution along the  $N/\Delta_v$  axis is equivalent to choosing a beam filling factor ( $\eta_{fill}$ ) for the clouds. Whereas it is justified to assume that the two lines share a common  $\eta_{fill}$ , its exact value in an external galaxy is unknown *a priori*. It is worth discussing to what extent our conclusions might depend on  $\eta_{fill}$ .

We have run LVG models for  $n(\text{H}_2)=5 \times 10^5 \text{ cm}^{-3}$  and  $T_k=50$ K, fitting  $R_{Tmb}=T_{mb}(\text{SiO})/T_{mb}(\text{H}^{13}\text{CO}^+)$  in the different regions of the CND. Table 1 fully explores the dependence of  $N(\text{SiO})/N(\text{H}^{13}\text{CO}^+)$  on  $\eta_{fill}$ ; the filling factor is varied within its whole range (0.005–1). The main conclusion, independent of  $\eta_{fill}$ , is that the SiO abundance is significantly enhanced in the outer CND (region **II**), where we derive  $N(\text{SiO})/N(\text{H}^{13}\text{CO}^+)=5-15$ , and contrary to what it might be expected, it is lower at the center and at the starburst ring **I**, where  $N(\text{SiO})/N(\text{H}^{13}\text{CO}^+)=1-2$ . The SiO abundance rises in the outflow, where we infer  $N(\text{SiO})/N(\text{H}^{13}\text{CO}^+)=3-5$ .

A density fall-off with radius has been reported by Wall et al. 1991 (and confirmed by Harrison et al. 1999). They concluded that  $n(\text{H}_2)$  might reach  $\sim 5 \times 10^4 \text{ cm}^{-3}$  for  $r > 20''$ , not far from region **II**. If we take  $n(\text{H}_2) \sim 5 \times 10^4 \text{ cm}^{-3}$ , we find that  $N(\text{SiO})/N(\text{H}^{13}\text{CO}^+)=20-100$  for **II**. Opacity in the 2–1 line of SiO is close to  $\sim 1$  for this solution, whereas  $\tau \sim 0.02$  for  $\text{H}^{13}\text{CO}^+$ . To fit the ratio of line temperatures we need imper-

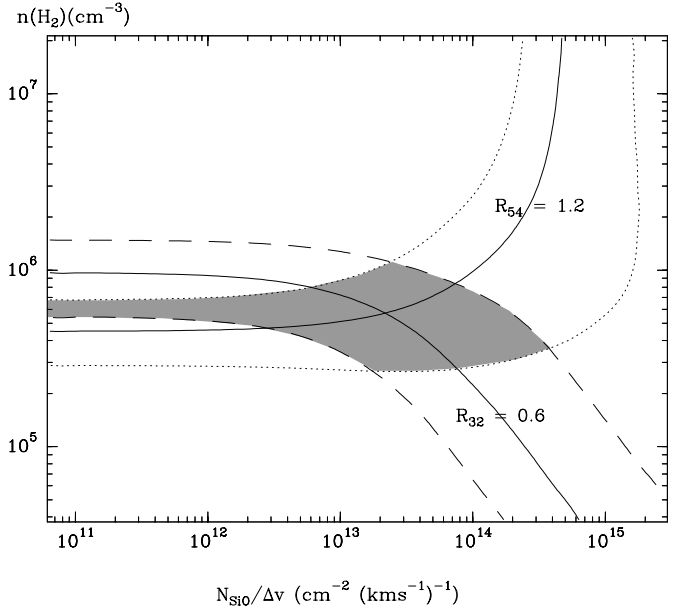


**Fig. 8.** This figure represents LVG solutions fitting the  $R_{54}=I(\text{SiO}(5-4))/I(\text{SiO}(3-2))$  and  $R_{32}=I(\text{SiO}(3-2))/I(\text{SiO}(2-1))$  line ratios (continuous lines) observed in the SiO clouds of the nucleus of NGC 253, assuming  $T=50$ K. We consider errors of 20% and 30% in ratios  $R_{54}$  and  $R_{32}$  (pointed and dashed lines delimit the region of allowed solutions within the errors tolerance). An average density of  $n(\text{H}_2)=5 \times 10^5 \text{ cm}^{-3}$  is a good compromise, indicating that the SiO emitting gas is dense. Trying to delimit further the LVG solution along the  $N/\Delta_v$  axis is equivalent to choose a beam filling factor ( $\eta_{fill}$ ) for the clouds.

atively to rise  $N(\text{SiO})/N(\text{H}^{13}\text{CO}^+)$  in region **II**. Consequently, conclusions on the SiO abundance enhancement of region **II** remain unchanged, if not clearly favoured, in the lower density scenario.

From the ratio  $N(\text{SiO})/N(\text{H}^{13}\text{CO}^+)$ , we can infer the absolute abundance of SiO ( $X(\text{SiO})=N(\text{SiO})/N(\text{H}_2)$ ), if we adopt a canonical value for  $\text{H}^{13}\text{CO}^+$  ( $\langle X(\text{H}^{13}\text{CO}^+) \rangle$ ). It is expected that SiO will be more sensitive than  $\text{H}^{13}\text{CO}^+$  to any varia-

tion of the chemical environment in NGC 253. This hypothesis is successfully confronted to the measurements of abundances of  $\text{H}^{12}\text{CO}^+$  obtained in a large variety of molecular clouds in our Galaxy where values close to  $10^{-8}$  are obtained in all cases (from which we derive  $X(\text{H}^{13}\text{CO}^+) \sim 10^{-10}$  if we adopt  $^{13}\text{C}/^{12}\text{C} \sim 1/90$ ). Though there is observational and theoretical evidence that  $X(\text{H}^{12}\text{CO}^+)$  may be reduced to  $10^{-10}$  in the hot cores of GMCs, SiO is lower by a similar factor in these sources (see Blake et al. 1987); moreover, very compact sources are not expected to dominate the emissivity of  $\text{H}^{13}\text{CO}^+(1-0)$  at the scale we are observing the nucleus of NGC 253. Contrary to  $X(\text{H}^{13}\text{CO}^+)$ ,  $X(\text{SiO})$  is measured to vary by several orders of magnitude in the Galaxy, depending on the type and the location of molecular clouds in the disk (see discussion). We can estimate  $\langle X(\text{H}^{13}\text{CO}^+) \rangle$  in the nucleus of NGC 253. From our data we obtain a column density of  $\langle N(\text{H}^{13}\text{CO}^+) \rangle = 3 \times 10^{12}$ , averaged within the CNB. Similarly, we can calculate  $\langle N(\text{H}_2) \rangle$  from the  $^{12}\text{CO}(1-0)$  map of Canzian et al. (1988), averaged on the same area. If we take the conversion factor  $x = N(\text{H}_2)/I_{\text{CO}} = 3 \times 10^{20} \text{ cm}^2 \text{ K km}^{-1} \text{ s}$ , it follows  $\langle N(\text{H}_2) \rangle \sim 3 \times 10^{22}$ , which implies global abundances of  $\langle X(\text{H}^{13}\text{CO}^+) \rangle \sim 10^{-10}$  in NGC 253, quite similar to the value inferred for our Galaxy.

Column 5 of Table 1 illustrates the variation of  $X(\text{SiO})$  in the CNB of NGC 253. We derive  $X(\text{SiO}) \sim 1-2 \times 10^{-10}$  for the center and the starburst ring **I**,  $X(\text{SiO}) \sim 5-15 \times 10^{-10}$  for region **II**, and  $X(\text{SiO}) \sim 3-5 \times 10^{-10}$  for the outflow. The global abundance of SiO in the CNB would be  $\langle X(\text{SiO}) \rangle \sim 1.5 \times 10^{-10}$ , namely, an order of magnitude above the typical value for a PDR (Janssen et al. 1995, Walmsley et al. 1999). Most notably,  $X(\text{SiO})$  reaches the highest abundance in the outer region **II**, where the chemical processing of the gas by the nuclear starburst, mostly ascribed to region **I**, should be minor. The SiO abundance is also significantly enhanced in the outflow, certainly powered by the starburst, but not directly on it. This result emphasizes that SiO emission is not always directly related to the dense gas near sites of recent star formation. Therefore, different mechanisms must be explored to account for the different chemical processing of molecular gas within the nucleus.

## 8. Discussion

We have established the existence of three distinct regions in the nuclear region of NGC 253, based on morphological, kinematical and chemical criteria. Region **I** dominates the global SiO emission and it is associated with the nuclear starburst taking place across  $\sim 150 \text{ pc}$ . It presents a ring-like pattern, interpreted as the gas response near the iILR of the bar. The SiO abundance in the starburst ( $X(\text{SiO}) \sim 1-2 \times 10^{-10}$ ) is significantly larger than that estimated for a typical PDR ( $X(\text{SiO-PDR}) \sim 10^{-11}$ ). Region **II** extending up to the map edges ( $r \sim 300 \text{ pc}(20'')$ ), displays a spiral-like morphology also present in other high-density tracers. The observed distribution and kinematics of molecular gas are interpreted as the signature of the bar oILR. The orbit crowding across the oILR coincides with the detection of strong non-circular motions ( $\Delta v \sim 50-100 \text{ km s}^{-1}$ ) and, most notably,

with an enhancement in the SiO abundance ( $X(\text{SiO}) \sim$  a few  $10^{-9}$ ). The third region constitutes the molecular counterpart of the nuclear gas outflow observed in X-ray and optical lines. This was recently identified as a dust chimney. Two filaments (N and S) come out of the plane of the NGC 253 nucleus from  $r \pm 60 \text{ pc}$ , near a working surface where the gas is entrained by the outflow. Again, we have found here a link between the existence of high-velocities ( $\Delta v \sim 100-150 \text{ km s}^{-1}$ ) and an SiO enrichment ( $X(\text{SiO}) > 3-5 \times 10^{-10}$ ).

Two processes are thought to dominate the chemistry of the molecular material associated with a starburst: the photodissociation of the gas by intense UV field produced by OB associations, and the existence of strong shock waves. Shocks can be generated locally during mass loss episodes in young stars (often identified as bipolar outflows). Alternatively, shocks may take place on a larger scale, either produced by supernova explosions or related to spiral/barred density waves. Contrary to  $X(\text{H}^{13}\text{CO}^+)$ ,  $X(\text{SiO})$  is measured to vary by several orders of magnitude in the Galaxy, depending on the type and the location of molecular clouds in the disk: star forming clouds ( $X(\text{SiO}) \sim 10^{-7}-10^{-8}$ ), galactic center clouds apparently not forming stars ( $X(\text{SiO}) \sim 10^{-9}$ ) or quiescent clouds ( $X(\text{SiO}) < 10^{-12}$ ).

It is well established that shocks occurring in bipolar outflows can enhance the abundance of SiO in the gas phase to reach, in the most extreme cases,  $\sim 10^{-7}$  (Martín-Pintado et al. 1992). Although the starburst region **I** might be described as a giant PDR (Carral et al. 1994), the relatively large abundances of SiO measured and the high densities of SiO clouds indicate that most of the emission arises in bipolar outflows powered by young massive stars, similarly to what is observed in the galactic complexes W51 and W49. Moreover, the particularly large ratio of  $I([\text{SiII}])/I([\text{OI}]) \sim 1$  measured in the inner region of NGC 253 indicates an enhancement of Si in gas phase. This was interpreted by Carral et al. 1994 as evidence of grain destruction in the starburst region, most likely by shocks related to massive star formation.

The case for shock processing is even stronger in region **II** and in the outflow where  $X(\text{SiO}) \sim (50-100) \times X(\text{SiO-PDR})$ . However, the origin of the large abundance of SiO in region **II** is less clear. SiO emission could arise partly in bipolar outflows powered by young massive stars like in region **I**. The major drawback to this explanation is that region **II** is located away from the nuclear starburst. Therefore one should not expect an enhancement of SiO when the chemical processing caused by star formation has declined. Alternatively, the SiO enhancement could be produced by large-scale shocks in the molecular gas, caused by the crossing of clouds orbits near the oILR of the bar. The only evidence for chemical enrichment of gas attributed to large-scale shocks is found in the Galactic Center where values of  $\sim 10^{-9}$  have been measured in SiO clouds (Martín-Pintado et al. 1997, Hüttemeister et al. 1998). However there is no theoretical consensus whether the shocks can be caused by the action of density waves, especially in molecular clouds. The hierarchy of fragmentation inhibits shocks in molecular clouds; the mean-free paths for cloud-cloud collisions are of the same order

of magnitude as the thickness of the disturbing potential well (Casoli and Combes 1982, Combes and Gerin 1985).

If the starburst scenario gives rise to SiO emission in bipolar outflows of young massive stars, the differences in the abundance of SiO in regions **I** and **II** might be explained if the starbursts are in a markedly different stage of evolution. The older starburst would occur in region **I**, where a large fraction of the young massive stars are already on the main sequence. The latter explains why the classical tracers of the starburst phenomenon are mostly restricted to **I**. In contrast, region **II** would contain a younger and less-evolved starburst, where most of the young massive stars would be still in the mass loss phase, characteristic of the pre-main sequence stage, where energetic bipolar outflows occur.

Finally, the interpretation of the morphology and kinematics of the molecular gas filaments give additional support to the outflow scenario. The enhancement of SiO in the gas phase observed in this region can be explained by the chemical processing of grains by the strong high-velocity shocks ( $v > 200 \text{ km s}^{-1}$ ) associated to the outflow.

*Acknowledgements.* This work has been partially supported by the Spanish CICYT under grant number PB96-0104.

## References

- Alton P.B., Davies J.I., Bianchi S., 1999, A&A 343, 51  
 Anantharamaiah K.R., Goss W.M., 1996, ApJ 466, L13  
 Antonucci R.R.J., Ulvestad J.S., 1988, ApJ 330, L97  
 Arnaboldi M., Capaccioni M., Cappellaro E., et al., 1995, AJ 110, 199  
 Athanassoula E., 1992, MNRAS 259, 328  
 Baan W.A., Bragg A.E., Henkel C., et al., 1997, ApJ 491, 134  
 Binney J., Gerhard O.E., Stark A.A., et al., 1991, MNRAS 252, 210  
 Blake G.A., Sutton E.C., Masson C.R., et al., 1987, ApJ 315, 621  
 Boker T., Krabbe A., Storey J.W.V., 1998, ApJ 298, L115  
 Buta R., Combes F., 1996, Fund. Cosmic. Physics 17, 95  
 Canzian B., Mundy L.G., Scoville N.Z., 1988, ApJ 333, 157  
 Carlstrom J.E., Jackson J., Ho P.T.P., et al., 1990, In: Hollenbach D.J., Thronson H.A. (eds.) The Interstellar Medium in External Galaxies. NASA Conf. Publ. 3084, p. 337  
 Carral P., Hollenbach D.J., Lord S.D., et al., 1994, ApJ 423, 223  
 Casoli F., Combes F., 1982, A&A 110, 287  
 Chini R., Reipurth B.O., Ward-Thompson D., et al., 1997, ApJ 474, 135  
 Combes F., 1994a, Nuclear Gas Flows in Barred Galaxies. In: Physics of the gaseous and stellar disks of the Galaxy. ASP Conference Series 66, p. 87  
 Combes F., 1994b, Role of resonances in ring formation. In: Combes F., Athanassoula E. (eds.) N-body problems and gravitational dynamics. p. 137  
 Combes F., Gerin M., 1985, A&A 150, 327  
 Demoulin M.H., Burbidge E.M., 1970, ApJ 159, 799  
 De Vaucouleurs G., 1958, ApJ 127, 487  
 Engelbracht C.W., Rieke M.J., Rieke G.H., et al., 1998, ApJ 505, 639  
 Fabbiano G., Trinchieri G., 1984, ApJ 285, 491  
 Fux R., 1998, In: The Physics and Chemistry of the Interstellar Medium. 3rd Cologne-Zermatt Symposium, Sep.1998, V.Ossenkopf Shaker-Verlag, Aachen, p. 91  
 García-Burillo S., Guélin M., 1995, A&A 299, 657  
 García-Burillo S., Combes F., Neri R., 1999, A&A 343, 740  
 Gueth F., Guilloteau S., Bachiller R., 1998, A&A 333, 287  
 Harrison A., Henkel C., Russell A., 1999, MNRAS 303, 157  
 Ho P.T.P., Martin R.N., Henkel C., Turner J.L., 1987, ApJ 320, 663  
 Hüttemeister S., Aalto S., 1998, In: The Physics and Chemistry of the Interstellar Medium. 3rd Cologne-Zermatt Symposium, Sep.1998, V.Ossenkopf Shaker-Verlag, Aachen, p. 80  
 Hüttemeister S., Dahmen G., Mauersberger R., et al., 1998, A&A 334, 646  
 Janssen D.J., Spaans M., Hogerheidje M.R., et al., 1995, A&A 303, 541  
 Krügel E., Chini R., Klein U., et al., 1990, A&A 240, 232  
 Martín-Pintado J., Bachiller R., Fuente A., 1992, A&A 254, 315  
 Martín-Pintado J., de Vicente P., Fuente A., et al., 1997, ApJ 482, L45  
 Martín-Pintado J., García-Burillo S., Fuente A., et al., 1999, A&A submitted, (MP99)  
 Mauersberger R., Henkel C., Sage L.J., 1990, A&A 236, 63  
 Mauersberger R., Henkel C., 1991, A&A 457, 466  
 Mauersberger R., Henkel C., Wielebinski R., et al., 1996, A&A 305, 421  
 McCarthy P.J., Heckman T., van Breugel W., 1987, AJ 92, 264  
 Olson K.M., Kwan J., 1990, ApJ 349, 480  
 Paglione T.A.D., Tosaki T., Jackson J.M., 1995, ApJ 454, L117  
 Peng R., Zhou S., Whiteoak J.B., et al., 1996, ApJ 470, 821, (P96)  
 Sage L., Ziurys L., 1995, ApJ 447, 625  
 Sams B.J. III, Genzel R., Eckart L., et al., 1994, ApJ 430, L33  
 Sandage A., Tammann G.A., 1975, ApJ 196, 313  
 Schilke P., Walmsley C.M., Pineau des Forêts G., et al., 1997, A&A 321, 293  
 Scoville N.Z., Soifer B.T., Neugebauer G., et al., 1985, ApJ 289, 129  
 Schulz H., Wegner G., 1992, A&A 266, 167  
 Tesesco C.M., Harper D.A., 1980, ApJ 235, 392  
 Turner B.E., 1985, ApJ 299, 312  
 Turner J.L., Ho P.T.P., 1985, ApJ 299, L77  
 Ulrich M., 1978, ApJ 219, 424  
 Ulvestad J.S., Antonucci R.R.J., 1991, AJ 102, 875  
 Wall W.F., Jaffe D.T., Israel F.P., et al., 1991, ApJ 380, 384  
 Walmsley C.M., Pineau des Forêts G., Flower D.R., 1999, A&A 342, 542  
 Watson A.M., Gallagher J.S.III, Holtzman J.A., et al., 1996, AJ 112, 534  
 Ziurys L.M., Friberg P., Irvine W.M., 1989, ApJ 343, 201